ISSN 1063-455X, Journal of Water Chemistry and Technology, 2018, Vol. 40, No. 4, pp. 219–227. © Allerton Press, Inc., 2018.

PHYSICAL CHEMISTRY
OF WATER TREATMENT PROCESSES

Performance and Morphology Evaluation of Thin Film Composite Polyacrylonitrile/Polyamide Nanofiltration Membranes Considering the Reaction Time[1]

M. Esmaeili[a, *], S. H. Mansoorian[b], A. Gheshlaghi[a], and F. Rekabdar[a]

[a]*Chemical, Polymeric and Petrochemical Technology Development Research Division, Research Institute of Petroleum Industry, Tehran, Iran*

[b]*Department of Chemical Engineering, University of Kashan, Iran*

**e-mail: majidesm2004@yahoo.com*

Received April 1, 2015

Abstract—Polyacrylonitrile/polyamide (PAN/PA) thin film composite nanofiltration membranes were manufactured by interfacial polymerization (IP) of trimesoylchloride reacting with piperazine, in the presence of triethylamine. The influence of IP reaction time up to 100 s on the membrane performance and structure was investigated considering flux, rejection, structural morphology and roughness of the membrane using permeation test, scanning electron microscopy, atomic force microscopy as well as fourier transform infrared spectroscopy. Structural evaluation of membranes revealed that the average PA surface pore size was reduced initially up to 60 s of reaction due to the crosslinking process and PA layer compaction increment, however, became larger at longer reaction times. The PA layer effective thickness grew up with IP time and became constant after 60 s. The best water flux and Na_2SO_4 salt rejection were obtained at 60 s of reaction, which were 100 m^3/day and 87% at pressure of 13 barg. Variation trends of permeation and morphological results showed accordance that confirmed their accuracy. Comparison of the Na^+ rejection value with the rejection of commercialized NF membrane of Dow Company (NF90-400/34i) showed acceptable result for membrane performance.

DOI: 10.3103/S1063455X18040070

Keywords: interfacial polymerization, polyamide, nanofiltration, composite membrane, reaction time.

INTRODUCTION

Polyacrylonitrile (PAN) membranes have attracted a great deal of attention amongst both academia and industrial researchers as UF-membrane due to its superior characteristics in hydrophilicity, solvent stability and cost effectivity. PAN membranes could offer great advantages as support of nanofiltration (NF) composite membranes, employed for rapidly expanding technologies such as water and wastewater treatment, desalination, etc. with rewards in reduction of membrane replacement cost and improved permeate quality [1–2]. Chemical treatment of nitrile groups (CN), among polymeric chains of PAN membrane, could be considered as a modification method in order to creation of desired properties such as antifouling and permeation improvement due to membrane hydrophilicity increment [3–4].

Interfacial polymerization (IP) is an important fabrication method for reverse osmosis (RO) and NF composite membranes preparation. In this method, a thin layer of polyamide (PA) film is attached on the support layer that is responsible for the separation performance. Potentials of IP procedure for fouling reduction of NF composite membranes have been investigated heretofore, which present some opportunities to optimize both the thin film properties and surface morphology of the support layer in order to achieve to the best overall separation performance and membrane stability [5–12]. Affective IP factors include monomers reaction time, concentrations, partition coefficients, overall kinetics and diffusion rates of reactants, reactivity ratio where blends of reactants are employed, polymer solubility in the solvent phase, presence of by-products, hydrolysis, cross linking, post treatment [13–23]. Ahmad and Ooi wrote a short literature review on the IP parameters under three distinct categories; preparation conditions, material selection and kinetic control [14–16]. The authors [24] in a study on the thin film composite (TFC) membranes, identified reaction time, relative humidity and coating temperature as the critical parameters and suggested their optimization for adjusting the membrane flux. In another work, the researchers [16] investigated the effects of reaction time on the surface pore size. They found that pore size reduces initially but later the pores tend to coalesce and become larger.

[1] The text was submitted by the authors in English.

Considering the significance of reaction time and the findings of [16] suggesting its potential optimization, in this article, the influence of IP reaction time on the performance of TFC-NF membranes is investigated considering flux, rejection, morphology and roughness of the membranes. Adjustment the performance and morphology of the PAN/PA composite membranes by changing the monomer reaction time is the focus of this study. Triethylamine (TEA) was used as a catalyst for IP reaction, which helped to reaction continuity and played an important role in changing the membrane surface morphology. The best IP reaction time for reaching to the industrial acceptable membrane performance based on the permeation and morphology analysis was evaluated. The mechanism of IP reaction and formation quality of PA layer was investigated carefully based on spectroscopic analysis.

EXPERIMENTAL

Materials

The PAN polymer (MW = 15000 Da) and its solvent N-methyl-2-pyrolidone (NMP) were obtained from Sigma-Aldrich Company for preparation of micro porous supports. PA active layer was built using piperazine (PIP) and trimesoyl chloride (TMC) as the monomers and TEA as the catalyst; the first two were purchased from Sigma-Aldrich, and the last from Merck Company. Feed solutes employed here include Na_2SO_4, $MgSO_4$ and NaCl; all of them were prepared from Merck.

Preparation of PAN Support Layer Through IP Method

PAN was first dried in an oven at 65°C for at least 5 h. Homogenized solution of PAN in NMP (20%, w/w) was poured onto a glass plate and casted with an applicator calibrated for 200 μm of film thickness. The glass plate was then immediately immersed in a water bath at room temperature in which it was maintained for 24 h to ensure full coagulation before being washed with de-ionized water.

Fabrication of PAN/PA TFC Membranes

PAN support membrane was mounted on a smooth glass plate and immersed into an aqueous amine solution containing PIP (2%, w/v) and TEA (0.45%, w/v) for 5 min at ambient temperature. Additional solution was removed from the PAN surface by applying a soft roller. A wooden frame was then clamped onto the glass plate before the organic solution containing TMC (0.3%, w/v) dissolved in *n*-hexane was poured onto the support within specified polymerization reaction times (selected to be 20, 40, 60 and 100 s) at 25°C. The nascent TFC membranes were then cured for 1 min at room temperature, before being washed with de-ionized water.

Membrane Characterization

Scanning electron microscopy analysis. Membranes surface and cross-section were examined using scanning electron microscopy (SEM) experiment. Samples were frozen in liquid nitrogen and fractured, before being sputtered with gold and evaluated with a Philips SEM apparatus at 5 kV acceleration voltages.

Atomic force microscopy analysis. Surface morphology and roughness of the membranes were investigated using a dual scope TM scanning probe-optical microscope AFM (DME model C-21, Denmark). Square of the prepared membranes were cut and glued on a glass substrate and viewed at scan size of 10 × 10 μm. Employing DME-SPM software, surface roughness parameters were obtained from the height profile of atomic force microscopy (AFM) images.

Fourier transform infrared spectroscopy. Presence of PAN and PA characteristic functional groups into the structure of support and active layer were analyzed by fourier transform infrared spectroscopy (FTIR) spectroscopy (IBB Bomem MB-100-Canada). This analysis was performed on the membrane samples in the range of 500 to 4000 cm^{-1} wave length with 10 cm^{-1} resolution.

Membrane performance testing. Permeation performance of PAN/PA composite membranes were tested with various feed solutions (1000 ppm aqueous solutions of Na_2SO_4, $MgSO_4$ and NaCl), using the NF test setup, capable of operating at various flow patterns, temperatures and pressures. A gear pump circulated the feed from temperature-controlled reservoir through the vertically aligned membrane unit with feed rated of 10 L/min. The retentate stream was returned to the feed reservoir. An electronic balance interfaced with a computer was used to collect permeated mass versus time data. Using a batch cross-flow system at 13 bar transmembrane pressures, the water flux and salt rejection of the membranes were measured by collecting the

permeate stream directly for 10 min after it had been stabilized for 60 min. All of the tests were repeated twice and the average value was reported for error reduction.

RESULTS AND DISCUSSION

Mechanism of IP Reaction between PIP and TMC

PIP is the simplest cyclic member of the ethylene amines family, which has two secondary amine groups and act both as a nucleophilic reagent in IP reaction and binder of PA layer to the PAN surface. TMC with three acyl functional groups (–COCl) is another active reagent in IP reaction that can easily react with water and generate carboxylic acid groups (–COOH). Acyl halides such as TMC (RCOX, X = halogen atom) react readily with water, alcohols, and amines and are widely used in organic synthetic processes whereby the acyl group is incorporated into the target molecules by substituting the acylation reaction, involving substitution by an electron donor group on the electrophilic carbonyl group (C=O) [21]. TEA is an acid scavenging catalyst due to the presence of two free electrons on its nitrogen atoms. This organic compound is more powerful acceptor of H^+ related to PIP during IP reaction.

IP reaction, which is so called self-limiting phenomenon, is diffusion-controlled and can be completed rapidly before the formation of a dense cross-linked barrier layer that prevents monomers to contact [16, 18, 22, 23, 25]. The polymer chains (PIP-TMC) are expected to contain both cross-linked and non-cross-linked structures containing carboxylic acid group. Due to the steric hindrance effect, one of the acyl groups of TMC may not readily react with PIpp. Instead of, one carboxylic acid functional group arises due to the partial hydrolysis [16, 23, 25–27]. Given time, the remaining acyl chloride groups, however, will undergo hydrolysis if no PIP is present [16, 25–31]. Generation of acid groups among PA chains increases the surface hydrophilicity and water permeation of composite membrane but diminishes cross-linking effect and salt rejection.

Evaluation of the PA Formation

Identifying the PA functional groups helps to clarify the effect of various reaction times on the PA structure [32]. FTIR spectroscopy was applied for this purpose, which related results has been demonstrated in Fig. 1, where a comparison can be made between different spectrums representing support PAN, pure PA polymer and prepared composite membranes with 20, 60 and 100 s of IP reaction times. The PA identification peaks will belong to the amide and acid carbonyl (C=O) bonds, which feature in the range of 1700–1725 cm^{-1} for acidic CO and 1640–1690 cm^{-1} for amide carbonyl. The carboxylic acid, if presents, will show a strong and broad bond covering the range between 3200 to 3600 cm^{-1} for the O–H stretch.

As can be seen in Fig. 1, the carbonyl stretching bonds have appeared in the range between 1650 to 1750, which the first at 1675 cm^{-1} belongs to the amide C=O and the next at 1730 belongs to the acidic C=O bonds. The important note is that the pure acyl chloride group (COCl) should present an absorbance peak for C=O stretch near 1800 cm^{-1}. However, there is not any sign of this peak on FTIR graphs of PA composite membranes. The PA composite membrane had been kept in dionized water after preparation according to section *Fabrication of PAN/PA TFC Membranes*. High tendency of acyl chloride to react in wet conditions and formation of carboxylic acid cause to disappear of carbonyl bonds of acyl halid and instead the acidic C=O has been appeared.

The peak near 2245 cm^{-1} is assigned to nitrile groups caused by triple stretching bond in PAN polymer in graphs *1*, *3*, *4* and *5* (see Fig. 1). This peak for a pure PAN polymer is more sharpener but the sharpness will be reduced for phase inversion PAN membranes due to the hydrolysis effect of aqueous nonsolvent and changing the C–N to the –COO groups [33]. The broad peak around 3400 cm^{-1} in graphs *3*, *4* and *5* is indicative of (–COOH) groups in the PA skin layer. Appearance of O–H stretch and amide and acidic carbonyl bonds related to COOH group in the spectrums *3*, *4* and *5* in comparison to the PAN support membrane (*1*) or PA polymer (*2*) (see Fig. 1) provides strong evidence that PA layer and PAN/PA composite membrane were formed. Moreover, the C=O and O–H peaks intensity of the PA composite membranes have increased when the reaction residence time is increased from 20 to 100 s, which shows that the number of amide functional groups and accordingly the thickness of the PA layer has enhanced.

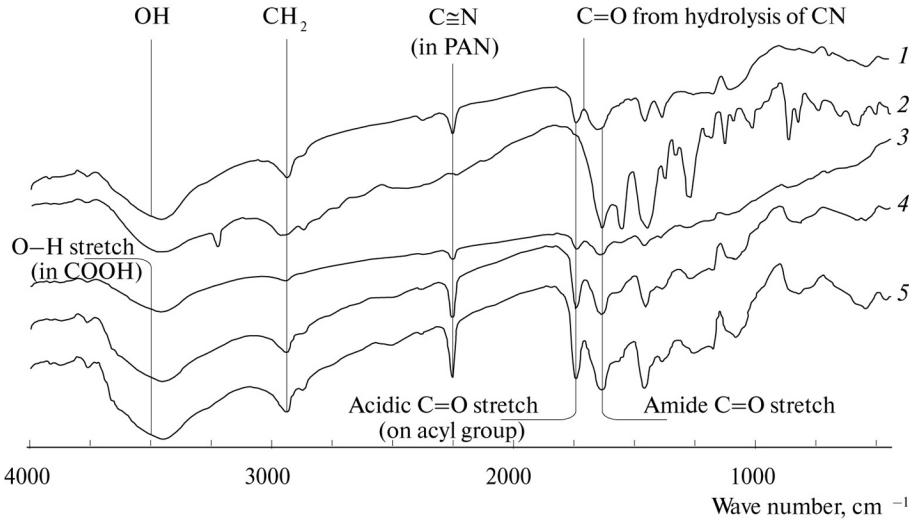

Fig. 1. FTIR spectrums for PAN support membrane (*1*), PA polymer (*2*), PA composite membranes (*3–5*) with 20, 60 and 100 s of IP reaction time.

Membrane Performance Analysis

Using 1000 ppm of Na_2SO_4 aqueous salt solution as feed at 13 bar operating pressure, salt rejection and permeability of the PAN/PA membranes were investigated with respect to the reaction time, which related results are shown in Fig. 2. There are interesting points regarding membrane performance at 60 s reaction time, indicating this to be the optimum reaction time. The feed flux was reduced about 23% from 130 to 100 L/(m^2·h) as reaction time progressed from 20 to 60 s, but followed with a lime descending trend afterwards up to 100 s. Na_2SO_4 rejection was increased about 40% from 20 to 60 s reaction time and reduced sharply to reach to the 43% of its maximum value. Both ascending and descending trends of flux and rejection, respectively in the first 60 s of reaction time confirm the formation and growth of the PA active layer. However, it could be expected to continue these trends after 60 s, but numerous repeated tests confirmed the results described changes after 60 s. This called for further investigations into the behavior of PA active layer, in which the morphology, roughness and pore size of the surface layer in association with the reaction mechanism were considered.

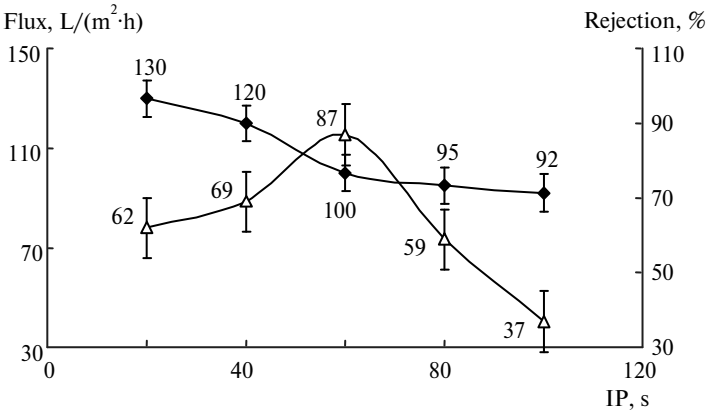

Fig. 2. Influence of IP reaction time on the TFC membrane performance using Na_2SO_4 in the feed solution (0.3% TMC, 2% PIP and 0.45% TEA).

Morphology Analysis

Using SEM analysis, both of the cross section and surface of the TFC fabricated membranes were investigated morphologically. The influence of various reaction times on the TFC membranes cross section can be observed in Fig. 3. Two distinguished layers of PA and PAN support can be identified, where the penetration progress of reacting monomers into the structure of PAN support membrane is visible. As reaction time increases, the structure of support membrane has been impressed more and the tips of pyramidal channels

become filled by the polymerization reaction products. More interestingly, the thickness of the PA active layer has been enhanced with increasing the reaction time from 20 to 60 s, where no further increase in the PA thickness is observed afterwards [21, 22, 31]. Using measuring tools in the SEM software, the average thickness of the PA active layers was measured across the cross sections, which has been plotted against IP reaction time in Table 1, which shows non-uniform increment rate for PA layer thickness [23, 31, 34]. It increased with slow gradient to 2.99 μm up to 20 s, then followed the ascending trend slightly afterwards between 20 and 60 s that reached to the maximum thickness after 60 s of reaction time (4.1 μm). Then the increment rate slowed down considerably to the extent that the thickness remained almost constant after 60 s.

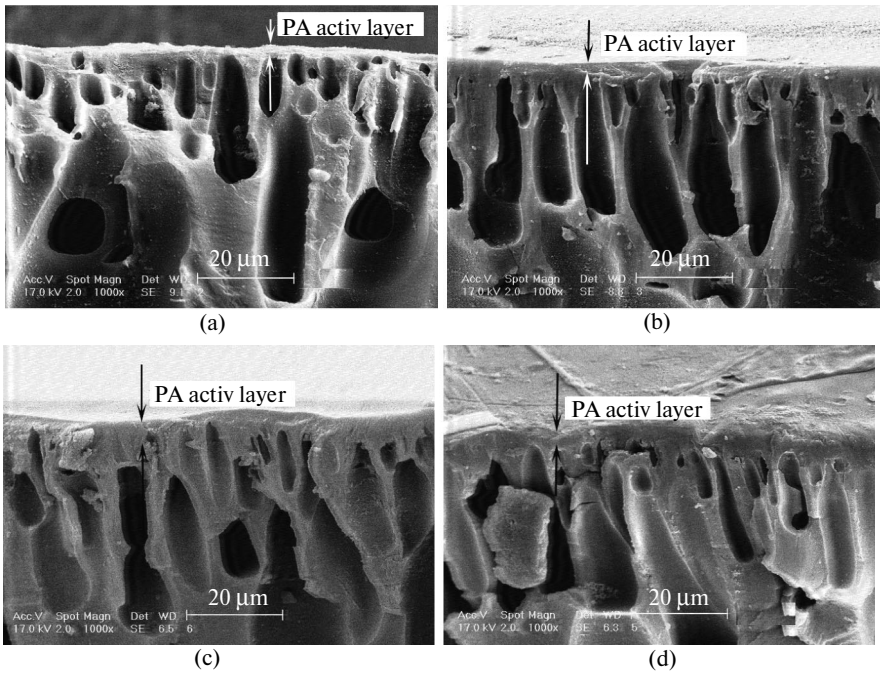

Fig. 3. SEM photographs from the cross section of TFC membranes with different reaction times, s: 20 (a), 40 (b), 60 (c) and 100 (d).

Table 1. Variation of PA active layer thickness against IP reaction time

Thickness, mc	IP, s
2.995	20
3.69	40
4.1	60
4.15	80

After soaking the support membrane into the PIP solution, the internal sections of the PAN structure is wetted by the diamine reagent. Therefore, both the surface and subsurface sections of the PAN membrane can be affected by the TMC solution. In the first 40 s of reaction, the TMC solution is capable of penetrate into the PIP encapsulated within internal voids of the PAN. Consequently, the influence of PA formation at the tips of pyramidal channels and internal structure of the PAN is visible in Fig. 3. After that, the created PA layer resisted against TMS penetration into the sub layers of formed PA layer. Consequently, no significant growth is observed in the thickness of the PA active layer after 60 s and polymerization reaction is impeded [32]. The permeation flux behavior presented in Fig. 2 is consistence with the growth pattern of PA active layer thickness described above. Interestingly, nearly constant flux corresponds to the constant thickness of the PA active layer after 60 s.

As regards the morphology of the surface, Fig. 4 illustrates the SEM images from the surface of the PA active layers prepared with different reaction times. Evidently, as reaction time progresses, the surface porosity seems to decrease up to the reaction time of 60 s (Figs. 5b, 5c) indicating the growth of the PA polymer chains, enlarging the clusters formed and reducing the interspaces between them. However, it is interesting to note that the surface porosity at 100 s of reaction time has increased slightly compared to the 60 s. This might

explain the very slight flux decrement and sever salt rejection reduction from 60 to 100 s of reaction time as seen in Fig. 2.

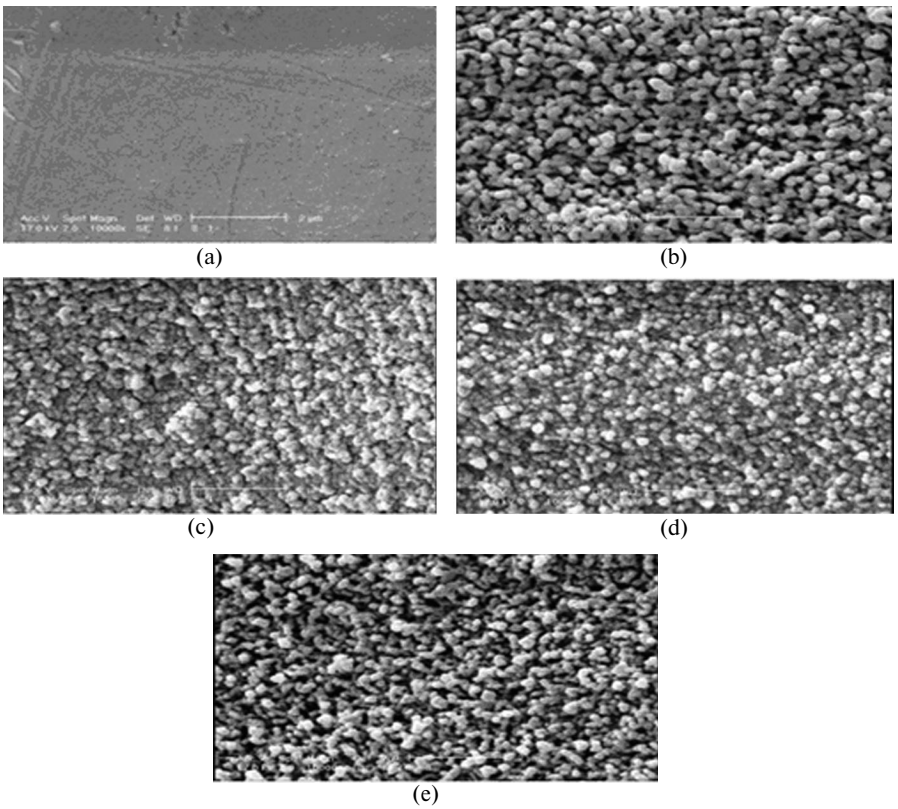

Fig. 4. SEM surface images of the TFC membranes for different reaction times, s: 0 (a), 20 (b), 40 (c), 60 (d) and 100 (e) (0 s corresponds to the PAN membrane).

Surface Roughness and Pore Size Analysis

Figure 5 illustrates the two and three dimensional AFM images of the TFC membranes. Roughness parameters and associated pore-size profiles within 100 μm^2 (10×10 μm) of the membrane were computed by the SPM-DME software which is presented in Table 2 and Fig. 5, respectively. R_y, R_z, R_a and R_q represent the interspace between the highest peak and lowest valley, mean distance between peaks and grooves, mean surface roughness and standard deviation for surface roughness, respectively [35–36].

According to Table 2 and Fig. 5, the roughness of the smooth PAN support (see Figs. 4, 5a) is lower than all of the PA layers roughness. The support membrane surface roughness has increased from 3.9 to 62.4 nm after 20 s of reaction time (see Fig. 4b) indicating the time lack for regular filling of PA chains produced within the PAN voids and its surface irregularities.

Table 2. Roughness parameters and mean pore size of the prepared membranes with different reaction times

Reaction, s	Mean pore size, nm	R_y	R_z	R_a	R_q
		nm			
0	700	32	30.3	3.92	4.83
20	200	561	550	62.4	80.3
60	110	545	465	20.4	31.6
100	300	1460	1160	47.8	71.3

Higher concentration of monomers at primary times of reaction causes to production of PA layers with higher rate at adjacent PAN surface position. Deposition of PA layers on the surface of PAN membrane and on each other takes places more homogeneously when the reaction rate is lower or reaction time is higher. Consequently, rougher surfaces are created when PA layers are produces with higher production rate at lower

reaction times. Upon reactants consumption, their concentration declines, thickness of PA layer increases on the surface and less reaction progress happens on the PAN surface. Therefore, the produced linear PA chains fill progressively the crystal lamellas, making the surface more homogeneous as reaction time increases to 60 s (see Fig. 5c), which causes to creation of smoother surface. However, the surface roughness increases up to 100 s of reaction time. This could be due to the non-uniform formation or irregular PA clusters, being left over the surface, thereby inhibiting appropriate contacts of TMC with the remaining PIP or water molecules on the surface. The height profile of AFM images that is computed by SPM-DME software has been shown also in Fig. 5 that enables the membrane mean pore size to be calculated as reported in Table 2 [19–21, 37]. The pore size was reduced from 700 to 110 nm when the reaction time increased from 0 to 60 s, respectively. However, further increment of reaction time up to 100 s has enlarged the pore size to 300 nm. These results conform to the morphological evidences presented by the SEM surface images at Fig. 4, where the surface compaction seems to have reduced for reaction time beyond 60 s. Also, the mentioned mean pore size confirms the rejection behavior of the membranes as presented in Fig. 2, where there is a considerable reduction in Na_2SO_4 salt rejection beyond 60 s of reaction time, corresponding to larger PA surface pore size.

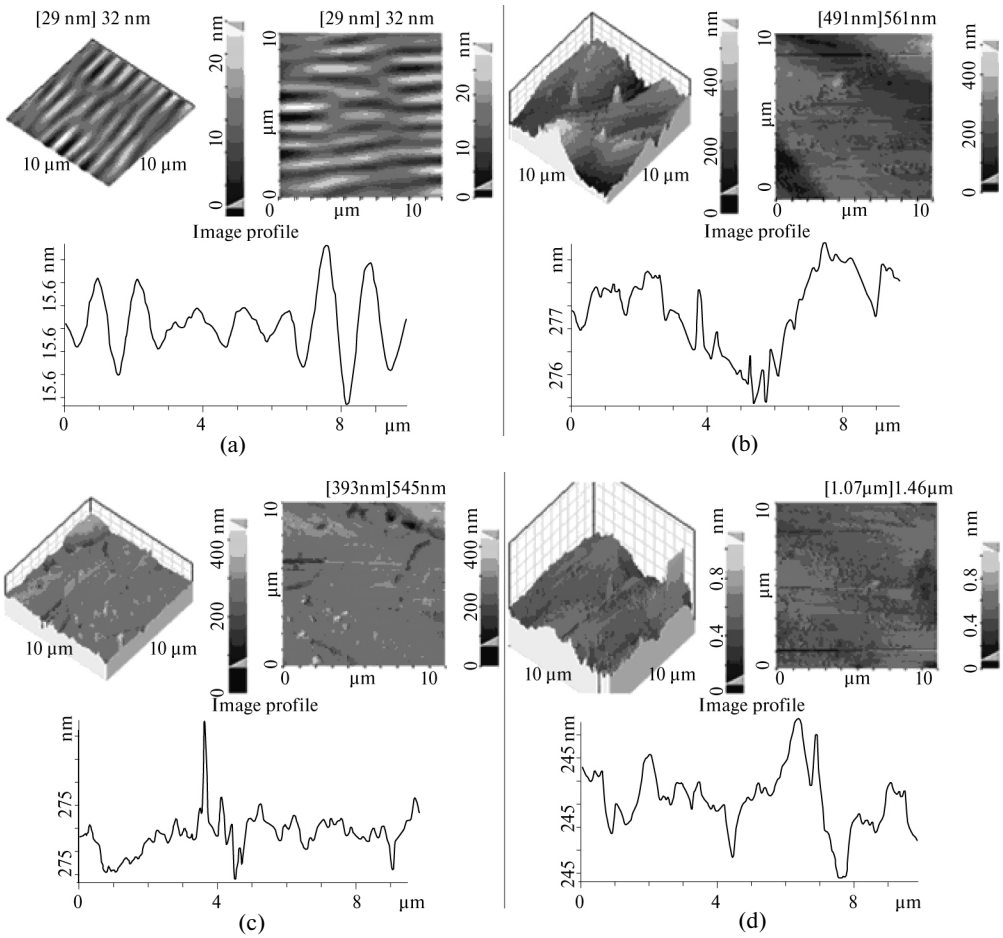

Fig. 5. Two and three dimensional AFM images and the associated pore-size profiles (polymerization times, s: 0 (a), 20 (b), 60 (c) and 100 (d)).

From the IP mechanism point of view these behavior could be interpreted as follow: as the IP reaction progresses, the PIP and TMC concentrations are reduced and skin layer thickness is increased, which leads to creation of more resistance against reaction of less available reactants. Water molecules in competition with the much-reduced PIP monomers start to react with TMC monomer that likely intensifies at 60 s of reaction time. TEA seeks to react with the resulting acidic hydrogen atom thereby promoting the IP reaction and leaving a highly polar product possessing N–H bond. This in-turn will attract polar water molecules toward the polar acyl chloride groups at the surface of created PA layer that is responsible for production of pores with weaker walls. The adjacent weaker pore walls would tend to coalesce together and create bigger pores at 100 s of reaction time.

Having found the optimized reaction time of 60 s for the membrane at 13 bar operating pressure, another same permeation test was carried at lower operating pressure of 8 barg, but at similar reaction time of 60 s. The results presented at Table 3, show similarity in rejection due to the similarity of the surface pore size at different pressures but indicate lower permeation rate for pure water at pressure of 8 barg because of the lower differential pressure across the membrane.

Table 3. The PAN/PA membrane performance results at two different operating pressures

$R_{Na_2SO_4}$, %	Flux for 37 m^2 membrane (like an industrial NF 8040 module, m^3/day)	Flux, m^3/day	Feed pressure, barg
87.5	42.62	48	8
87	88.8	100	13

Finally, in order to investigate the water hardness reduction performance of the PAN/PA membranes, permeation tests were repeated using $MgSO_4$ and NaCl salts at the similar Na_2SO_4 concentration and operating pressure that results are presented in Fig. 6. The highest and lowest salt rejection is related to Na_2SO_4 and NaCl salts, respectively with the maximum and minimum ionic size. The results shows that the effect of salt type on the rejection property of the membrane is stronger that on the water fluxes. Consequently, the TFC membrane is effectively capable to salt rejection and could be classified as the nanofiltration membrane suitable for treating slightly salty water.

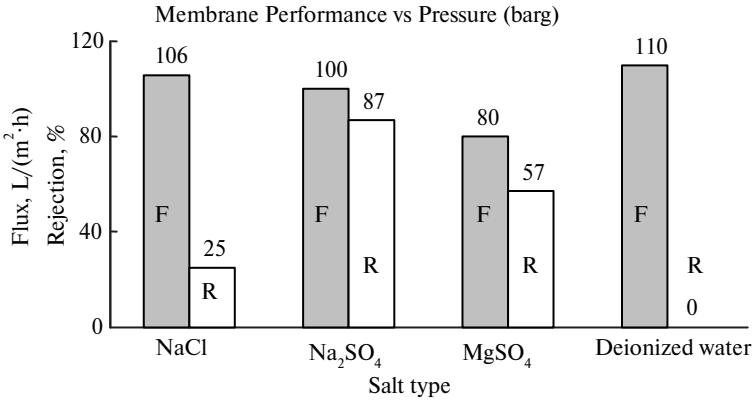

Fig. 6. Comparison of the water flux and hardness reduction performance of the TFC membranes.

CONCLUSIONS

Adjustment the preparation parameters of the PAN/PA thin film composite nanofiltration membrane considered in this study to investigate the influence of the IP reaction time on the membrane performance on the basis of the flux, rejection, morphology and roughness of the membrane. The SEM analysis revealed that among the four IP reaction times of 20; 40; 60 and 100 s, the PA thickness increases up to the 60 s due to the penetration potency of TMC and PIP monomers toward each other among created PA layer and performing the IP reaction. After that up to 100 s of reaction, resistance of the created PA layer and reduction of monomers concentration prevent from reaction progress and thereby slow the polymerization reaction and eventually cease the PA layer growth. On the other hand, consumption of the acidic hydrogen atoms by TEA groups leads to further absorption of water molecules toward membrane surface that causes to hydrolysis of TMC molecules making them inactive. The water molecules, which are drawn inside the pores, apply pressure and weaken the pores walls and lead to their breakage and enlargement of the surface pore size. The best membrane performance obtained at 13 barg for the membrane prepared by 60 s of reaction time. Na_2SO_4 salt rejection and pure water flux of 87 and 100 L/(m^2·h) were attained, respectively for this membrane which is acceptable for industrial applications. The salt rejection is 10% lower than industrial cases (FILMTEC NF90-400/34i Nanofiltration Element) however; the pure water flux is 48% higher than.

REFERENCES

1. Nghiem, L.D. and Schäfer, A.I., *Desalination*, 2006, vol. 187, pp. 303–312.
2. Martinetti, C.R., Childress, A.E., and Cath, T.Y., *J. Membrane Sci.,* 2009, vol. 331, pp. 31–39.

3. Bryjak, M., Hodge, H., and Dach, B., *Die Angewandte Makromol. Chem.*, 1998, vol. 260, pp. 25–29.
4. Oh, N.-W., Jegal, J., and Lee, K.-H., *J. Appl. Polym. Sci.*, 2001, vol. 80, pp. 2729–2736.
5. Raghuraman, L., *Desalination*, 1993, vol. 91, pp. 155–163.
6. Sanders, F.E. and Lozier, J.C., *Ibid.*, 1995, vol. 103, pp. 133–145.
7. Mänttäri, M., Nuortila-Jokinen, J., and Nyström, M., *J. Membrane Sci.*, 1997, vol. 137, pp. 187–199.
8. Koyuncu, I. and Yazgan, M., *J. Environ. Sci.*, A, 2001, vol. 36, pp. 1321–1333.
9. Sridhar, S., Prasad, K.K., Murthy, G.S., et al., *J. Chem. Technol. and Biotechnol.*, 2003, vol. 78, pp. 1061–1067.
10. Joshi, S.V., Ghosh, P.K., Shah, V.J., et al., *Desalination*, 2004, vol. 165, pp. 201–208.
11. Turan, M., *Ibid.*, 2004, vol. 170, pp. 83–90.
12. D.J. Xu, P., Bellona, C., Amy, G., et al., *Water Environ. Res.*, 2005, vol. 77, pp. 40–48.
13. Petersen, R.J., *J. Membrane Sci.*, 1993, vol. 83, pp. 81–150.
14. Ahmad, A.L. and Ooi, B.S., *Separ. and Purif. Technol.*, 2006, vol. 50, pp. 300 ¬ 309.
15. Ahmad, A.L. and Ooi, B.S., *Ibid.*, 2006, vol. 47, pp. 162–172.
16. Ahmad, A.L., Ooi, B.S., Wahab Mohammad, A., and Choudhury, J.P., *J. Appl. Polym. Sci.*, 2004, vol. 94, pp. 394–399.
17. Saha, N.K. and Joshi, S.V., *J. Membrane Sci.*, 2009, vol. 342, pp. 60–69.
19. Mansourpanah, Y., Madaeni, S.S., Adeli, M., et al., *J. Appl. Polymer Sci.*, 2009, vol. 112, pp. 2888–2895.
20. Mansourpanah, Y., Madaeni, S.S., and Rahimpour, A., *Separ. and Purif. Technol.*, 2009, vol. 69, pp. 234–242.
21. Mansourpanah, Y., Madaeni, S.S., and Rahimpour, A., *J. Membrane Sci.*, 2009, vol. 343, pp. 219–228.
22. Mansourpanah, Y., Madaeni, S.S., Rahimpour, A., and Farhadian, A., *Appl. Surface Sci.*, 2009, vol. 255, pp. 8395–8402.
23. Mansourpanah, Y., Madaeni, S.S., Rahimpour, A., et al., *J. Membrane Sci.*, 2009, vol. 330, pp. 297–306.
24. Prakash Rao, A., Joshi, S.V., Trivedi, J.J., et al., *Ibid.*, 2003, vol. 211, pp. 13–24.
25. Ahmad, A.L. and Ooi, B.S., *Ibid.*, 2005, vol. 255, pp. 67–77.
26. Jegal, J., Min, S.G., and Lee, K.-H., *J. Appl. Polym. Sci.*, 2002, vol. 86, pp. 2781–2787.
27. Odian, G. *Principles of polymerization*, New Jercy: John Wiley and Sons, 2004, 812 p.
28. Zimmermann, R., *Angew. Chem. Int.,* 1966, vol. 5, no. 8, pp. 749–750.
29. Janssen, L.J.J.M. and te Nijenhuis, K., *J. Membrane Sci.*, 1992, vol. 65, pp. 69–75.
30. Aharoni, S.M., *Polym. Adv. Technol.*, 1995, vol. 6, pp. 373–382.
31. Liu, J.-Q., Xu, Z.-L., Li, X.-H., et al., *Separ. and Purif. Technol.*, 2007, vol. 58, pp. 53–60.
32. Madaeni, S.S., Esmaeili, M., Attar Nosrati, S., and Barzin, J., *Int. Polym. Proc.*, 2013, vol. 28, pp. 281–290.
33. Li, W., Yang, Z., Zhang, G., et al., *J. Mater. Chem.*, *A*, 2014, vol. 2, pp. 2110–2118.
34. Song, Y., Liu, F., and Sun, B., *J. Appl. Polym. Sci.*, 2005, vol. 95, pp. 1251–1261.
35. Esmaeili, M., Madaeni, S.S., and Barzin, J., *Separ. and Purif. Technol.*, 2013, vol. 103, pp. 289–305.
36. Esmaeili, M., Madaeni, S.S., and Barzin, J., *Polym. Int.*, 2010, vol. 59, pp. 1006–1013.
37. Rahimpour, A., Madaeni, S.S., Shockravi, A., and Ghorbani, S., *J. Membrane Sci.*, 2009, vol. 334, pp. 64–73.